Insights into quasi solid-state polymer electrolyte

Liu, Zelin; Zhang, Shu; Zhou, Qian; Zhang, Yidong; Lv, Dong; Shen, Yanghuan; Fu, Xiangnan; Wang, Xinyi; Luo, Shiyu; Zheng, Yun; Peng, Yu; Chai, Jingchao; Liu, Zhihong; Cui, Guanglei

Published in:
Battery Energy

DOI:
10.1002/bte2.20220049

Published: 01/05/2023

Document Version
Final published version

Document License
CC BY

Received: 26 September 2022 | Revised: 27 October 2022 | Accepted: 1 November 2022

DOI: 10.1002/bte2.20220049

RESEARCH ARTICLE

BATTERY ENERGY Open Access WILEY

Insights into quasi solid-state polymer electrolyte: The influence of succinonitrile on polyvinylene carbonate electrolyte in view of electrochemical applications

Zelin Liu[1] | Shu Zhang[2] | Qian Zhou[2] | Yidong Zhang[3] | Dong Lv[4] | Yanghuan Shen[1] | Xiangnan Fu[1] | Xinyi Wang[1] | Shiyu Luo[1] | Yun Zheng[1] | Yu Peng[1] | Jingchao Chai[1] | Zhihong Liu[1] | Guanglei Cui[2]

[1]Key Laboratory of Optoelectronic Chemical Materials and Devices (Ministry of Education), Jianghan University, Wuhan, China

[2]Qingdao Industrial Energy Storage Technology Institute, Qingdao Institute of Bioenergy and Bioprocess Technology, Chinese Academy of Sciences, Qingdao, China

[3]Laboratory of Natural Materials Technology, Åbo Akademi University, Turku, Finland

[4]Department of Biomedical Sciences, City University of Hong Kong, Kowloon Tong, Hong Kong, China

Correspondence
Jingchao Chai and Zhihong Liu, Key Laboratory of Optoelectronic Chemical Materials and Devices (Ministry of Education), Jianghan University, Wuhan 430056, China.
Email: chaijc@jhun.edu.cn and liuzh@jhun.edu.cn

Guanglei Cui, Qingdao Industrial Energy Storage Technology Institute, Qingdao Institute of Bioenergy and Bioprocess Technology, Chinese Academy of Sciences, Qingdao 266101, China.
Email: cuigl@qibebt.ac.cn

Funding information
National Natural Science Foundation of China, Grant/Award Numbers: 51872127, 22139001; Key R&D Plan of Hubei Province, Grant/Award Number: 2020BAA030; Chutian Scholar Program of Hubei Province.

Abstract

Quasi solid-state composite polymer electrolytes have generated much interest due to their high ionic conductivity and stable interfacial compatibility with electrodes. However, they suffer from the balance of liquid plasticizer content and ionic conductivity to retard potential safety issues. In this paper, a polyvinylene carbonate (PVCA)-based quasi solid-state composite polymer electrolyte for ambient-temperature lithium-ion battery is proposed, wherein succinonitrile (SN) serves as the multifunctional component to increase the ionic conductivity. The study indicates that SN can plasticize the polymer electrolyte, coordinate with lithium-ion, and modulate the molecular weight of the polymer. The fabricated PVCA–SN polymer electrolyte delivers an ionic conductivity up to 4.5×10^{-4} S/cm at 25°C. The assembled lithium-ion battery based on PVCA electrolyte demonstrates an excellent rate performance and high-capacity retention at ambient temperature. The proposition of PVCA-based quasi solid-state composite polymer electrolyte provides a resultful strategy for high-performance rechargeable lithium batteries.

KEYWORDS
in situ polymerization, lithium-ion battery, polymer electrolyte, polyvinylene carbonate, succinonitrile

1 | INTRODUCTION

To address the increasingly depleted energy problem and the gradual deterioration of the ecological environment, a series of energy-saving, emission-reduction, green and low-carbon measures have been introduced. Lithium-ion batteries have come out on top in the field of energy storage equipment in recent decades due to their high energy density, reliable cycle performance, and pollution-free characteristics.[1] Recently, with the continuous updating of technology, there is an urgent need for next-generation batteries.[2] Specifically, with flammable and potentially dangerous liquid electrolytes in most commercial lithium-ion batteries, safety issues such as spontaneous combustion and explosions of new energy vehicles occur frequently.[3] The electrolyte is called the blood of lithium batteries, establishing a bridge connecting the cathode and anode.[4] A high-performance electrolyte is required to have excellent electrochemical properties and reliable safety.[5] Commercial liquid electrolytes exhibited high ionic conductivity, and wide electrochemical window; however, the safety of liquid electrolytes needs to be improved. To elevate the safety of lithium-ion batteries, solid electrolytes with low flammability, nonvolatility, and mechanical and thermal stability were widely developed.[1d,6]

Normally, solid electrolytes can be classified into two categories, including all solid electrolytes and quasi solid electrolytes (QSSEs).[7] Despite the high safety, all solid electrolytes have distinct limitations. For instance, oxide electrolytes have poor flexibility and inferior interface resistance, sulfide electrolytes suffer from a narrow electrochemical window and the shuttle effect,[8] and halide electrolytes with high sensitivity to water and oxygen have restricted requirements to the environment.[9] Alternatively, solid-state polymer electrolytes composed of polymer matrix and lithium salt show advantages over inorganic electrolytes,[1d,10] including processability, flexibility, and interfacial compatibility. However, their ionic conductivity at ambient temperature ($<10^{-5}$ S/cm) is low which severely limits their utilization. Compared to all solid-state electrolytes, QSSEs have generated much interest due to their high ionic conductivity, stable interfacial compatibility with electrodes, and reliable safety.[7a,11] QSSE is essentially a kind of gel polymer electrolyte but with lower content of liquid plasticizers. Due to the weak synergistic effect between plasticizer molecules and polymer matrix, gel polymer electrolytes usually possess lots of liquid organic molecules. For example, previous studies reported polyvinylene carbonate (PVCA) based gel polymer electrolytes with a high liquid organic molecule content of 40%.[12] To further reduce the potential safety issues of gel polymer electrolytes caused by liquid organic molecules, it is highly desirable to develop QSSEs with optimized content of solid plasticizer to obtain high ionic conductivity.

Here, we proposed a PVCA-based quasi solid-state composite polymer electrolyte by simply introducing succinonitrile (SN) served as the multifunctional component to enable ambient-temperature lithium-ion batteries. The fabricated PVCA–SN polymer electrolyte delivered a high ionic conductivity of 4.5×10^{-4} S cm^{-1} at 25°C, and presented good interfacial compatibility with electrodes. We attribute this high performance to the synergistic effect between SN and PVCA. In addition, the PVCA-based battery presented a good rate of performance and high-capacity retention. The proposition of PVCA-based quasi solid-state composite polymer electrolyte provides an available strategy for high-performance rechargeable lithium-ion batteries.

2 | EXPERIMENTAL SECTION

2.1 | General

Compounds vinylene carbonate (VC), SN, and 2,2-azobisisobutyronitrile(AIBN) were purchased from Aladdin or Macklin. Compound lithium difluoro(oxalato) borate (LiDFOB) was obtained from Fosai New Material. Compound VC was purified by column chromatography with neutral Al_2O_3 in the glove box. The other compounds were used directly without any further purification. The cellulose nonwoven (NKK 4030, 30 μm) was purchased on Shenshenlicai. $LiFe_{0.31}Mn_{0.69}PO_4$ (LFMP) was supported by the Qingdao Institute of Bioenergy and Bioprocess Technology, Chinese Academy of Sciences.

2.2 | Preparation of solid-state polymer electrolyte and electrodes

The solvent of VC/SN was prepared in an Ar-filled glovebox. Then, 1 M LiDFOB was dissolved in the mixed solvent. The thermal initiator, AIBN, was added to the mixed solution at a concentration of 5 mg/ml. The solution was heated at 60°C for 24 h under Ar protection and the PVCA–SN–LiDFOB electrolyte was obtained. For the composited polymer electrolyte, cellulose nonwoven served as the support materials in cells. The designed PVCA–SN–LiDFOB/cellulose composite polymer electrolyte was abbreviated to PVCA–SN CPE. The LFMP cathode was composed of LFMP active material, Ketjen black, and LA133 binder with a weight rate of 8:1:1. The areal loading of active material in the LFMP electrode was about 2 mg/cm^2. The graphite anode was composed

of graphite, Ketjen black, CMC binder, and SBR binder with a weight rate of 8:1:0.5:0.5. The areal loading of active material in the graphite electrode was about 2 mg/cm^2.

2.3 | Sample characterization

The morphology of the samples was characterized by a field emission scanning electron microscope (SU8010; Hitachi). The mechanical property was investigated by an Instron-3300 universal testing machine (UTM2503; Sunstest) at a stretching speed of 10 mm/min. The FTIR spectra of the membranes are conducted using the attenuated total reflection attachment on a Frontier FTIR spectrometer (TENSOR27; Bruker) in transmission mode. Differential scanning calorimetry (DSC; Q20, TA) was carried out to measure the thermal properties of the polymer electrolyte from −80°C to 100°C at a heating rate of 10°C min^{-1} under a nitrogen atmosphere. X-ray diffraction (XRD) (X'Pert Powder; Panalytical) were recorded in the range of 5°–90°. Data were collected with a step width of 0.01°.

To calculate the residual ratio of VC, a certain amount of PVCA–SN polymer electrolyte was dissolved in dimethylformamide (DMF), and then poured into a PTFE culture dish. The whole sample was vacuum dried at 50°C for 3 days. Compound VC will volatilize with DMF and result in a mass loss of the system. The residual ratio of VC can be calculated by the ratio of mass loss to initial VC mass.

2.4 | Electrochemical measurements and battery tests

The assembly method of all batteries was similar to the liquid electrolyte-based batteries, but the cellulose separator was substituted for the commercial PP separator. The LiDFOB/VC/SN/AIBN solution was injected into the batteries before polymerization. The assembled batteries were heated at 60°C for 24 h, followed by the cooling process to ambient temperature. The assembly process of batteries was similar to the liquid electrolyte-based batteries. For the LFMP/PVCA–SN CPE/Li batteries, the batteries were galvanostatically charged to 4.35 V and kept at 4.35 V for 0.5 h, followed by a galvanostatically discharge process to 2.5 V. Before preparation of LFMP/PVCA–SN CPE/Li batteries, graphite/liquid electrolyte/Li batteries were firstly precycled for 10 times at 0.1 C, and then disassembled. The pre-cycled graphite electrode served as the anode in tLFMP/PVCA–SN CPE/Li battery. For the LFMP/PVCA–SN CPE/graphite batteries, the batteries were galvanostatically charged to 4.2 V and kept at 4.2 V for 0.5 h, followed by a galvanostatically discharge process to 2.5 V.

2.5 | Calculation methods

All structure optimizations and energy calculations were performed by Gaussian 09 package at B3LYP/6-311+G (d,p) level.

3 | RESULTS AND DISCUSSION

3.1 | Physical characteristics of PVCA–SN polymer electrolyte

The preparation diagram of the PVCA–SN polymer electrolyte was displayed in Figure 1A. Compound VC could polymerize under the initiation of AIBN (Figure 1B). At a low VC volume content (20%), the obtained electrolyte was fluid with a certain viscosity (Supporting Information: Figure S1 and Table S1). The viscosity increased with the increased volume content of VC. Quasi solid-state electrolytes were achieved when the VC volume content was up to 60%. Hence, the system with a VC volume content of 60% was chosen as the research object in the rest of this article, unless indicated otherwise. It should be noted that the color of VC/SN systems changed to sienna from transparent after the polymerization process. However, the change was not delivered in PC/SN systems or VC/SN systems without AIBN (Supporting Information: Figure S2). In this paper, LiDFOB was chosen as the lithium salt in the electrolyte. It has been reported that LiDFOB has a high decomposition temperature of up to 240°C,[13] which has been used as a lithium salt in polymer electrolytes.[6a,12] In addition, the LiDFOB-based electrolytes have shown excellent electrochemical performance and their cells delivered improved cycling performance at high temperatures and good safety characteristics owing to the combined advantages of LiBOB and $LiBF_4$. Here, a PVCA/SN/LiDFOB mixed solution in DMF was also transparent even after the heating process (Supporting Information: Figure S3). Therefore, it could be deduced that SN acted as a chain transfer agent during the polymerization process of VC. To study the mechanism of polymerization, three samples of VC/LiDFOB/AIBN, VC/SN/AIBN, and VC/SN/LiDFOB/AIBN were heated at 60°C for 24 h. As can be seen from Figure 1C, the obtained PVCA/LiDFOB was transparent, and PVCA/SN was light yellow. The three achieved samples were dissolved in DMF and then washed with abundant deionized water and ethanol, respectively. The rinsing process was repeated five times to completely

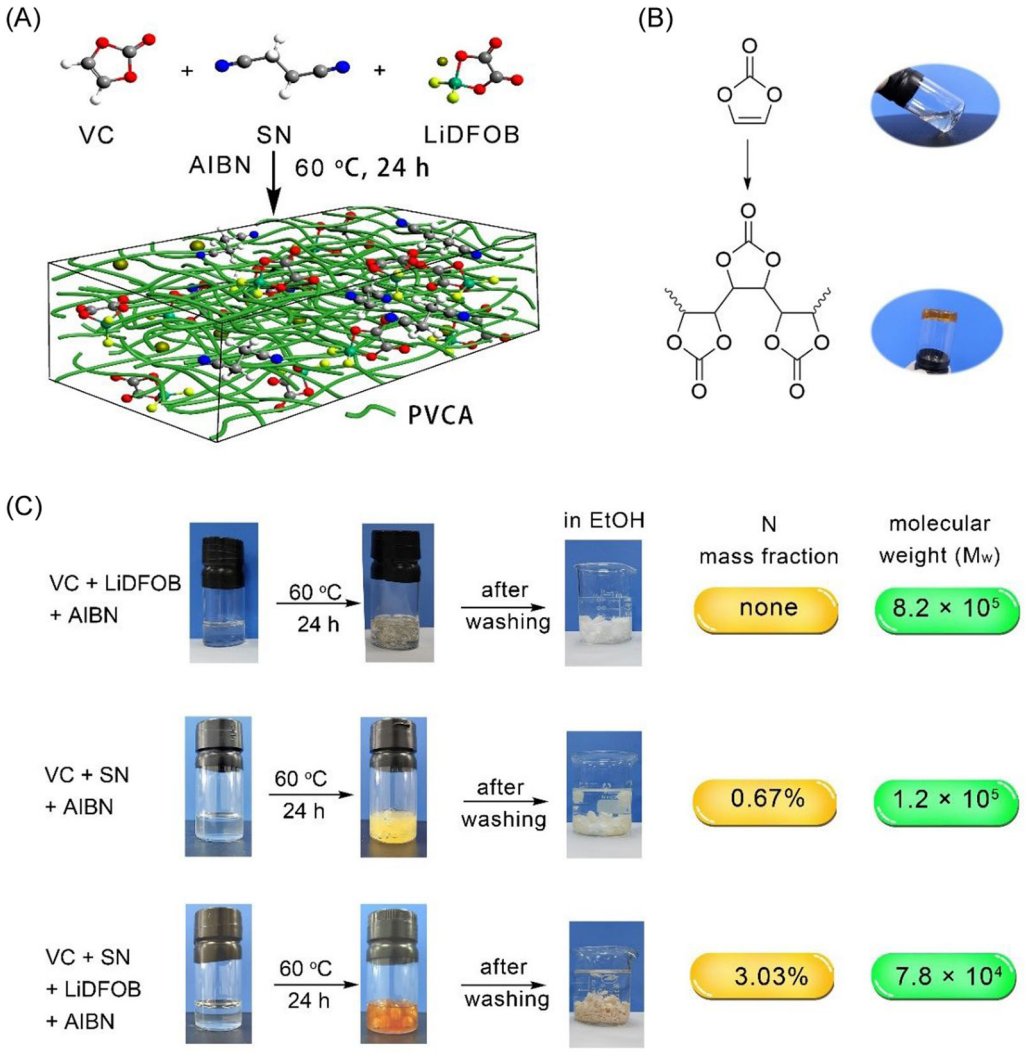

FIGURE 1 (A) Reaction diagram of PVCA–SN electrolyte. (B) Polymerization mechanism of VC. Inserts were pictures of the electrolyte before and after the heating process. (C) Digital photographs of three samples before and after polymerization. AIBN, 2,2-azobisisobutyronitrile; EtOH, ethanol alcohol; LiDFOB, lithium difluoro(oxalato)borate; PVCA, polyvinylene carbonate; SN, succinonitrile; VC, vinylene carbonate.

remove DMF and SN. Pure PVCA was white, the polymer in PVCA/SN was also white but with a very light yellow, and the polymer in PVCA/SN/LiDFOB was light sienna. The elemental analyzer test indicated that the N mass fraction in the polymer in PVCA/SN was 0.67% and that in PVCA/SN/LiDFOB was 3.03%. It was observed that the absence of LiDFOB could induce more SN to take part in the reaction. In addition, SN and LiDFOB could also decrease the molecular weight of the polymer (Supporting Information: Figure S4). For convenience, the designed polymer was also referred to as PVCA due to the relatively low content of the N element.

As the polymer electrolyte is obtained from in situ polymerization process, the support material is indispensable to separate the cathode and anode. In this paper, the cellulose nonwoven (NKK4030, 30 μm) was chosen as the support material due to the abundant 3D porous channels less than 2 μm in diameter (Supporting Information: Figure S5) and high wettability to the liquid electrolyte (Supporting Information: Figure S6). Benefitting from these properties, cellulose nonwoven has been widely used as the supporting material for polymer electrolytes,[2c,6a,12,14] including all solid-state electrolytes and gel polymer electrolytes. The cellulose-composited PVCA–SN polymer electrolyte was abbreviated to PVCA–SN CPE. The photograph of PVCA–SN CPE was shown in Supporting Information: Figure S7. The PVCA–SN CPE was translucent with a light sienna. The surface scanning electron microscopy (SEM) image (Supporting Information: Figure S8) showed that the PVCA–SN polymer electrolyte was fully infiltrated into the 3D porous channels of cellulose nonwoven.

Compound SN is a kind of plastic crystal, which has been widely applied in polyethylene oxide-based polymer electrolytes.[15] In the XRD pattern, SN presented two

crystallization peaks at 19.9° and 28.1° (Figure 2A). Pure PVCA exhibited a broad diffraction peak at ~20°, revealing the amorphous nature of PVCA. The proposed PVCA–SN–LiDFOB presented a similar XRD pattern to PVCA, and no SN crystallization peaks were found. The amorphous structure was beneficial to improve the ionic conductivity of electrolytes. From the Fourier-transform infrared spectroscopy (FT-IR) of varied samples, it can be found that PVCA–SN–LiDFOB presented a superimposed spectrum, arising from PVCA, SN, VC, and LiDFOB (Figure 2B). The absorption peaks at 1823 and 1791 cm^{-1} came from the C═O vibration band. The absorption peaks at 2982, 2250, and 1426 cm^{-1} were related to SN. Additionally, a new infrared absorption peak at 2356 cm^{-1} was presented in the sample of PVCA–SN–LiDFOB (Supporting Information: Figure S9). Hu et al.[16] believed that the interactions of C≡N···Li^+ would offset the FT-IR of C≡N to a higher wave number side, revealing that SN could also assist in the transference of lithium ions in electrolytes. It should be noted that a small peak at 3163 cm^{-1} was displayed in PVCA–SN–LiDFOB, which was from unsaturated ═C–H vibration band of VC, revealing that unpolymerized VC molecules still remained in PVCA–SN polymer electrolyte. After calculation, the PVCA–SN polymer electrolyte was composed of SN (32.6 wt.%), unreacted VC (19.8 wt.%), and PVCA (47.6 wt.%) except LiDFOB (Figure 2C, calculation method is shown in the Experimental section). This result was also verified by ^{1}H NMR spectra (Supporting Information: Figure S10). As we know, VC is a common additive in liquid electrolytes, which can participate in the formation of solid-electrolyte interfacial membranes on the cathode and anode.[17] A small number of VC is in favor of upgrading the cycling performance of batteries.

The thermodynamic properties of PVCA–SN polymer electrolytes can be evaluated by DSC. The DSC curve of SN delivered two melting peaks at −35.5°C and 58.8°C

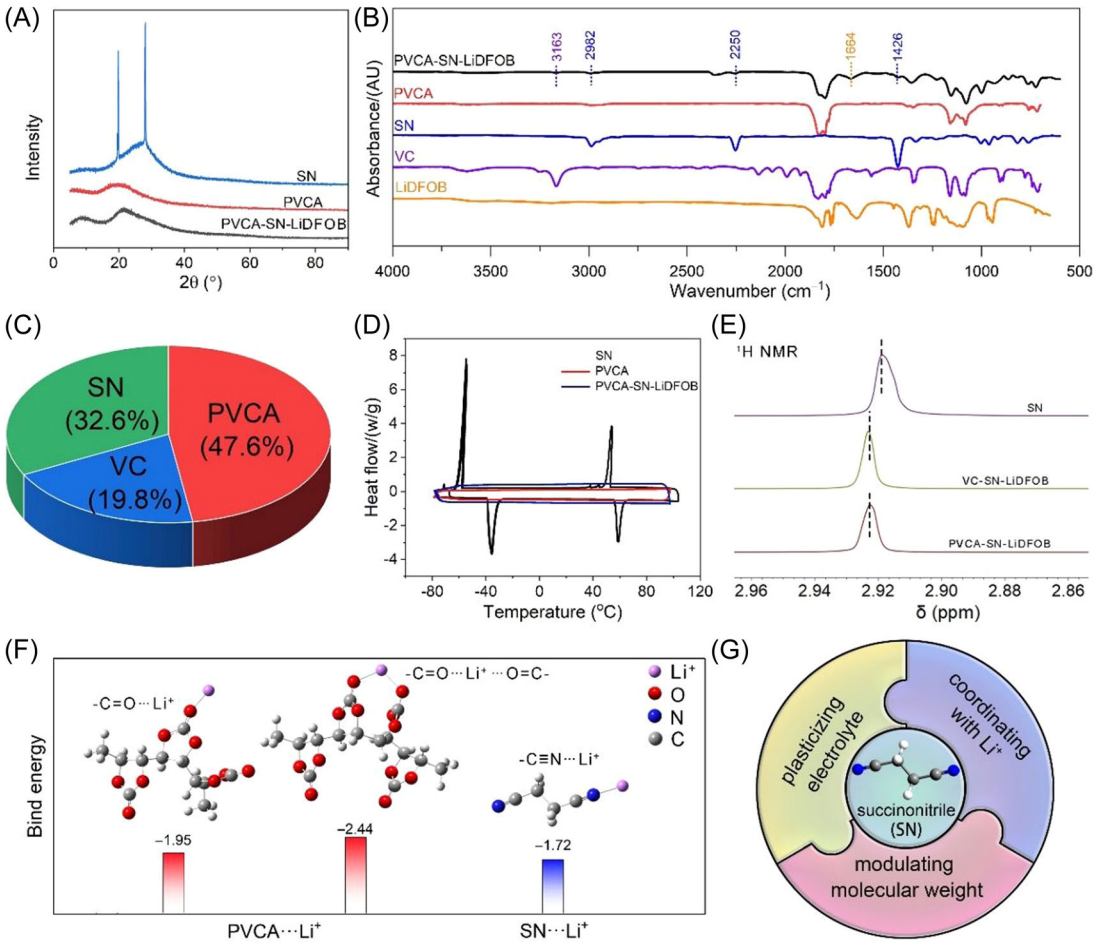

FIGURE 2 Physical characterization of PVCA–succinonitrile (SN) CPE. (A) XRD and (B) FT-IR of varied samples. (C) Composition, (D) DSC, and (E) 1H NMR of PVCA–SN–LiDFOB with 60% VC. (F) Bind energy of lithium ions to PVCA and SN. (G) Three major functions of SN in PVCA–SN CPE. CPE, composite polymer electrolyte; DSC, differential scanning calorimetry; FT-IR, Fourier transform infrared; LiDFOB, lithium difluoro(oxalato)borate; NMR, nuclear magnetic resonance; PVCA, polyvinylene carbonate; VC, vinylene carbonate; XRD, X-ray diffraction.

(Figure 2D). Crystalline SN shows plasticity in this temperature range. However, no melting peak was displayed in PVCA and PVCA–SN polymer electrolyte samples, implying that the SN was dispersed in the polymer electrolyte, which was in agreement with the XRD result. In *N*,*N*-dimethyl-d_6-formamide, the interaction between SN and Li^+ would shift the ^1H NMR signal of $-CH_2$ to a lower magnetic field due to the inductive effect of Li^+ (Figure 2E). To study the interaction quantitatively, density functional theory was applied to calculate the binding energy of lithium ions to PVCA and SN. The binding energy between one Li^+ and one carbonate group was −1.95 eV (Figure 2F and Supporting Information: Table S2), and it would become −2.44 eV when one Li^+ was complexed with two adjacent carbonate groups. In contrast, the binding energy between one Li^+ and one cyano group was −1.72 eV, indicating that Li^+ was prone to bind to PVCA. Given the above, compound SN played three important roles (Figure 2G): (1) plasticizing the polymer electrolyte; (2) coordinating with lithium-ion; and (3) modulating the molecular weight. The three functions could accelerate the transference of lithium ions in electrolytes.

3.2 | Electrochemical properties of PVCA–SN polymer electrolyte

Compared with liquid electrolytes, polymer electrolytes usually delivered a lower ionic conductivity, limiting their application in high-power density batteries. Hence, the ionic conductivity of polymer electrolytes is generally considered to be one of the most important parameters. The ionic conductivity of samples with varied volume content of VC before and after polymerization was evaluated at ambient temperature. In the liquid state (before polymerization), all samples demonstrated a closed ionic conductivity between 6.4 and 7.2 mS/cm (Figure 3A). However, the corresponding polymer electrolytes (after polymerization) showed a huge difference. The sample without SN could be identified as an all solid-state polymer electrolyte with an ionic conductivity of 9×10^{-7} S/cm. The low ionic conductivity was not satisfied in the operating condition of the lithium batteries at ambient temperature. With increased SN content, the polymer electrolytes exhibited an increased ionic conductivity due to multiple effects of SN as mentioned above. The sample with 60% SN content exhibited the highest ionic conductivity of 5.3×10^{-4} S/cm at 25°C due to its liquid state (Supporting Information: Figure S11). The relatively low ionic conductivity of the sample with 80% SN content was attributed to the lower solubility of LiDFOB in electrolytes. The sample with 40% SN content, namely 60% VC content, exhibited a relatively higher ionic conductivity of 4.5×10^{-4} S/cm at 25°C.

In consideration of the interactions between lithium ion and PVCA/SN in QSSEs, the transference mechanism of lithium-ion could be summed as the following three aspects: (1) $-C{\equiv}N\cdots Li^+\cdots N{\equiv}C-$; (2) $-C{=}O\cdots Li^+\cdots O{=}C-$; (3) $-C{\equiv}N\cdots Li^+\cdots O{=}C-$ (Figure 3B). Multiple synergistic effects of SN induced the rapid transference of lithium-ion in PVCA–SN CPE. The temperature-dependent conductivity of PVCA–SN CPE (with 60% VC content) was shown in Figure 3C. PVCA–SN CPE delivered an ionic conductivity of 4.5×10^{-4} S cm^{-1} at 25°C, close to the reported PVCA gel polymer electrolyte (5.6×10^{-4} S cm^{-1}).[12] The relationship between ionic conductivity and temperature can be fitted by the Vogel–Tamman–Fulcher empirical equation: $\sigma = AT^{1/2}\exp(-E_a/(R(T-T_o)))$, where A is the conductivity pre-exponential factor, which is related to the number of carrier ions, E_a is the activation energy for conduction corresponding to polymer segmental mobility, and T_o is a temperature which is related to the glass transition temperature. The fitting curve was depicted as the red line in Figure 3C. The ion transference activation energy of PVCA–SN CPE was 0.034 eV, which was only half as much as that of PVCA gel polymer electrolyte with carbonates,[12] indicating that the ion transference barrier in PVCA–SN CPE was lower than that in PVCA gel polymer electrolyte. We attribute this to the relatively lower conjugation between lithium-ion and SN than that between lithium-ion and carbonate ester.

As we know, SN and VC can react with lithium metal, especially at high temperatures (Supporting Information: Figure S12). The reaction of VC would generate PVCA, avoiding the contact of SN with lithium. A piece of lithium metal was placed in liquid VC/SN with 60% VC. No obvious change was found before and after the heating process (Supporting Information: Figure S12a), indicating that the hypothesis was right. Hence, the VC–SN–LiDFOB electrolyte could directly contact lithium metal, enabling the operability for the next experiment. The interfacial impedance of Li/Li symmetric battery was first studied. The assembled Li/PVCA–SN CPE/Li symmetric battery delivered an interfacial impedance of 548 Ω at ambient temperature (Supporting Information: Figure S13). The interfacial impedance decreased with galvanostatic polarization cycles at a current density of 0.2 mA/cm^2 and kept at about 90 Ω after the following cycles. This phenomenon was also found in liquid electrolyte-based Li/Li symmetric batteries.[18] The decreased interfacial impedance was related to the surface morphology of lithium metal electrodes during the lithium-ion plating/stripping process.[19] Time-dependent interfacial impedance was also

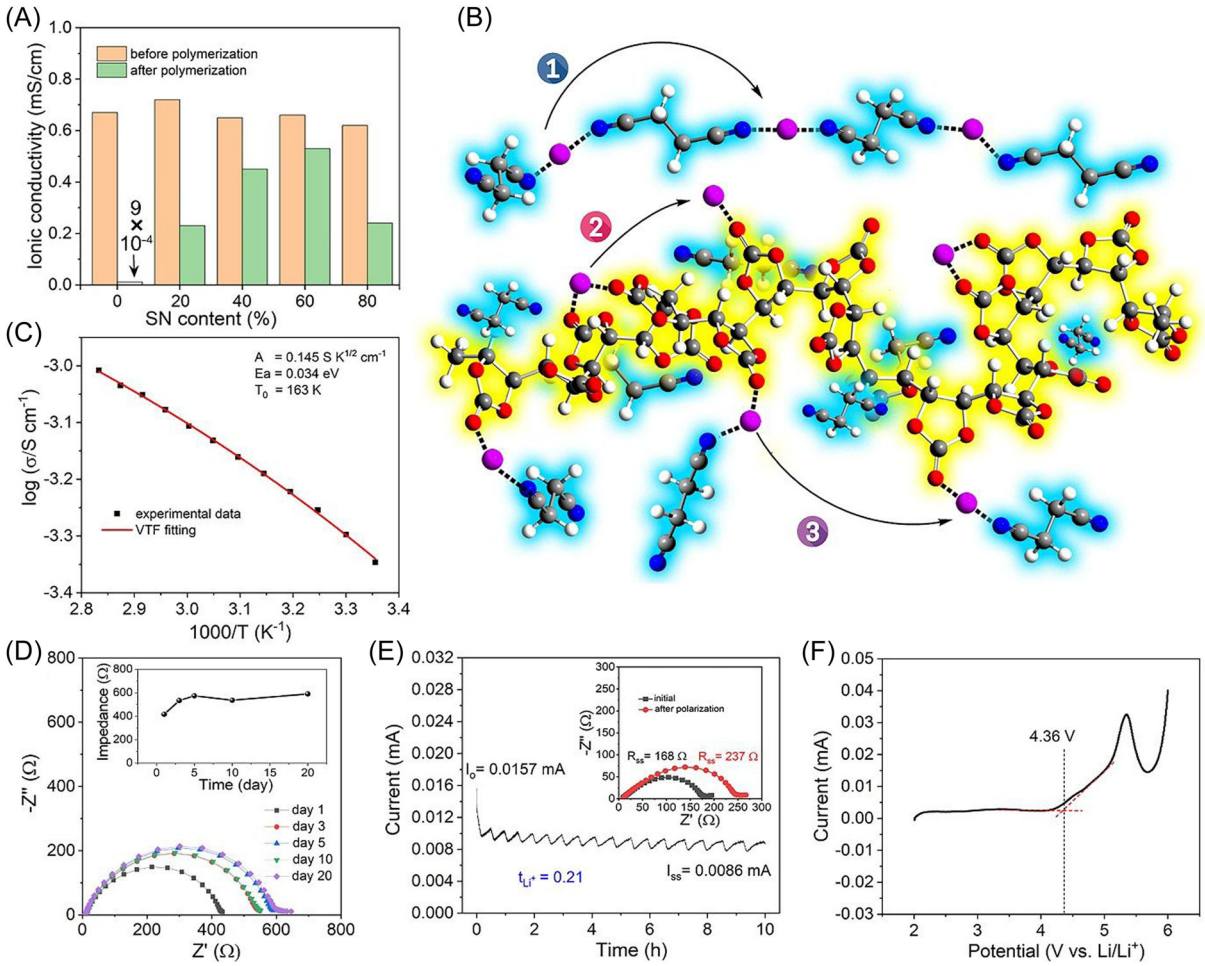

FIGURE 3 Electrochemical properties of PVCA–SN CPE. (A) Ionic conductivity of systems with varied VC volume content before and after polymerization. (B) Three transference mechanisms of lithium-ion in PVCA–SN CPE. The purple balls represent lithium ions. The molecules with blue and yellow light were SN and PVCA, respectively. (C) Temperature-dependent ionic conductivity of CPE at varied temperatures. (D) Time-dependent interface impedance of lithium metal asymmetric cells assembled with PVCA–SN CPE. (E) Current–time curve following a DC polarization of 0.003 V of Li/Li symmetric battery. (F) Linear sweeping voltammetry curve of Li/PVCA–SN CPE/SS asymmetrical cell at 25°C. CPE, composite polymer electrolyte; PVCA, polyvinylene carbonate; SN, succinonitrile; SS, stainless steel; VC, vinylene carbonate; VTF, Vogel–Tamman–Fulcher.

monitored by EIS. The Li/Li symmetric battery exhibited an increased interfacial impedance at first and was kept at ~530 Ω without an obvious increase (Figure 3D) in 20 days.

Lithium-ion transference number (t_{Li^+}) presented the contribution of the lithium-ion to the overall ionic conductivity, which was a key parameter for electrolytes.[20] In lithium-ion batteries, the effective ion was lithium cation, and the transference of the corresponding anion would increase the polarization during the charging/discharging process of batteries. The t_{Li^+} can be calculated from the Bruce–Vincent–Evans equation and the results are shown in Figure 3E. The impedance of the Li/Li symmetric battery before polarization was 168 Ω. After chronoamperometry at 3 mV for 10 h, the symmetric battery showed an impedance of 217 Ω. Hence, the calculated t_{Li^+} was 0.21, which was lower than the gel polymer electrolyte.[12] The decreased t_{Li^+} was possibly ascribed to the strong interaction between Li^+ and carbonate (Figure 2F). The complexation between the carbonate group and Li^+ was advantageous to dissolve lithium salt, but also limited the transference of Li^+ in the electrolyte.

As a functional component for lithium-ion batteries, the electrolyte was sandwiched between the cathode and anode. The cathode had a high potential and the anode had a low potential when the battery was fully charged. Therefore, electrolytes should possess excellent oxidative resistance and reducing resistance. Linear voltammetry sweep scan demonstrated that PVCA–SN CPE has an oxidative potential of 4.36 V (vs. Li/Li^+) (Figure 3F), which was slightly lower than PVCA-based gel polymer

electrolyte.[12] The decreased oxidative potential may be due to the existence of residual VC. Nevertheless, PVCA–SN CPE possesses the potential to match with most cathode electrodes.

3.3 | Charge/discharge performance of PVCA–SN polymer electrolyte-based batteries

In this paper, a phosphate electrode with the olivine structure, $LiFe_{0.31}Mn_{0.69}PO_4$ (LFMP), served as the cathode. Compared with $LiFePO_4$, LFMP presented an increased energy density, due to the higher redox potential of Mn^{2+}. Hence, LFMP delivered a huge potential in high energy density lithium batteries. The assembled LFMP/PVCA–SN CPE/Li battery delivered a stable charge/discharge performance at current densities of 1 and 2 C (Figure 4A). The LFMP/PVCA–SN CPE/Li battery presented two obvious charge/discharge platforms at 3.5 and 4.1 V (Figure 4B), corresponding to the CV results (Supporting Information: Figure S14). To simulate the application of PVCA–SN CPE in large-scale energy storage devices, pouch batteries were obtained by in situ polymerization process. The designed battery was shown in Figure 4C. As can be seen from the charge/discharge curves, the discharge capacity of the battery was 64.8 mAh at a current of 5 mA (Figure 4D). The charge/discharge curves were similar to those in button cells with two platforms at 3.5 and 4.1 V. At the charge state, the pouch battery can light the red LED sign of "JHUN," which presented the authors' affiliation with Jianghan University (Figure 4E). As we know, polymer electrolyte-based lithium batteries usually delivered a high safety performance. As expected, LFMP/PVCA–SN CPE/Li soft package battery could light the LED sign even after being cut three times.

A lithium-ion full battery, wherein LFMP and graphite served as the cathode and anode, respectively, was produced via in situ polymerization process. The assembly diagram of the LFMP/PVCA–SN CPE/graphite battery was shown in Figure 5A. The battery galvanstatically charged to 4.2 V and kept at 4.2 V for 0.5 h, and then galvanstatically discharged to 2.5 V. The assembled LFMP/PVCA–SN CPE/graphite battery showed a reversible discharge capacity of 150.1, 146.0, 141.4, 138.3, 133.9, 131.5, 129.6, 125.6, and 121.9 mAh/g at 0.5 C, 1 C, 2 C, 3 C, 4 C, 5 C, 6 C, 8 C, and 10 C, respectively (Figure 5B). As can be seen from Figure 5C, at the low current density, LFMP/PVCA–SN CPE/graphite battery presented two obvious charge/discharge platforms at 3.2 and 3.9 V. However, the charging platform related to Mn^{2+}/Mn^{3+} became indistinct with the increased current density, due to the polarization effect. In spite of

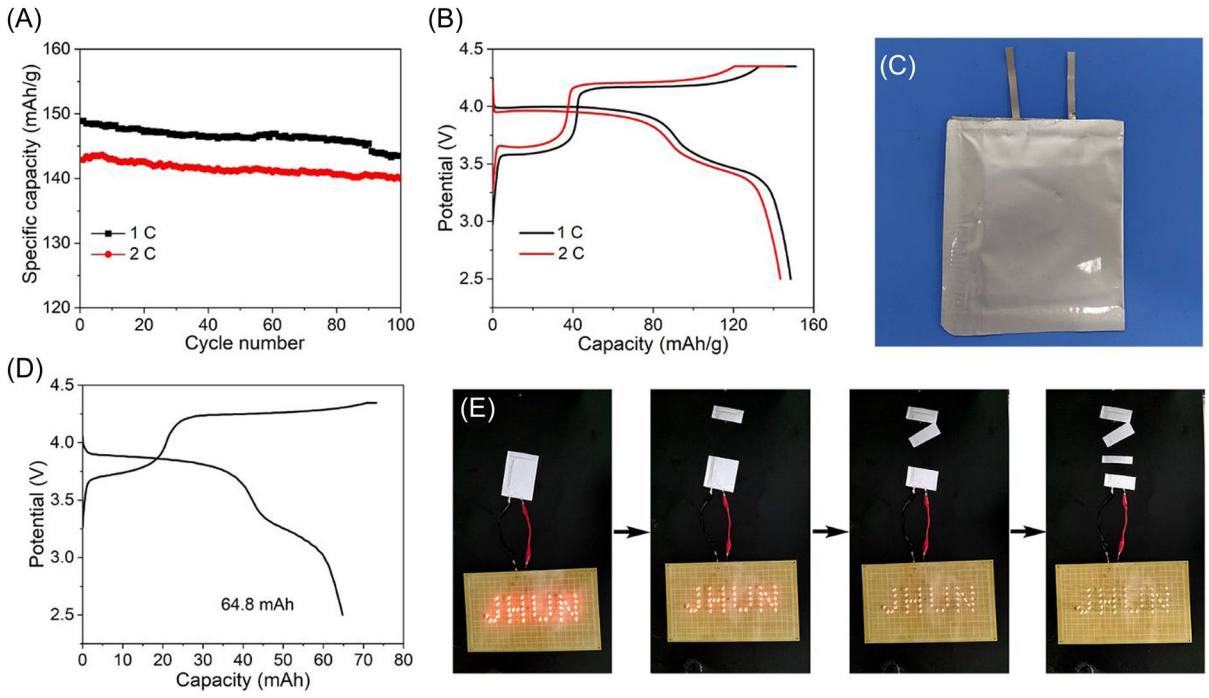

FIGURE 4 (A) Long cycling performance and (B) charge/discharge curve of LFMP/PVCA–SN CPE/Li battery at 1 and 2 C. (C) Digital photograph of pouch battery. (D) Charge/discharge curves of soft package battery at a current of 5 mA. (E) Cutting test of soft package battery. CPE, composite polymer electrolyte; LFMP, $LiFe_{0.31}Mn_{0.69}PO_4$; PVCA, polyvinylene carbonate; SN, succinonitrile.

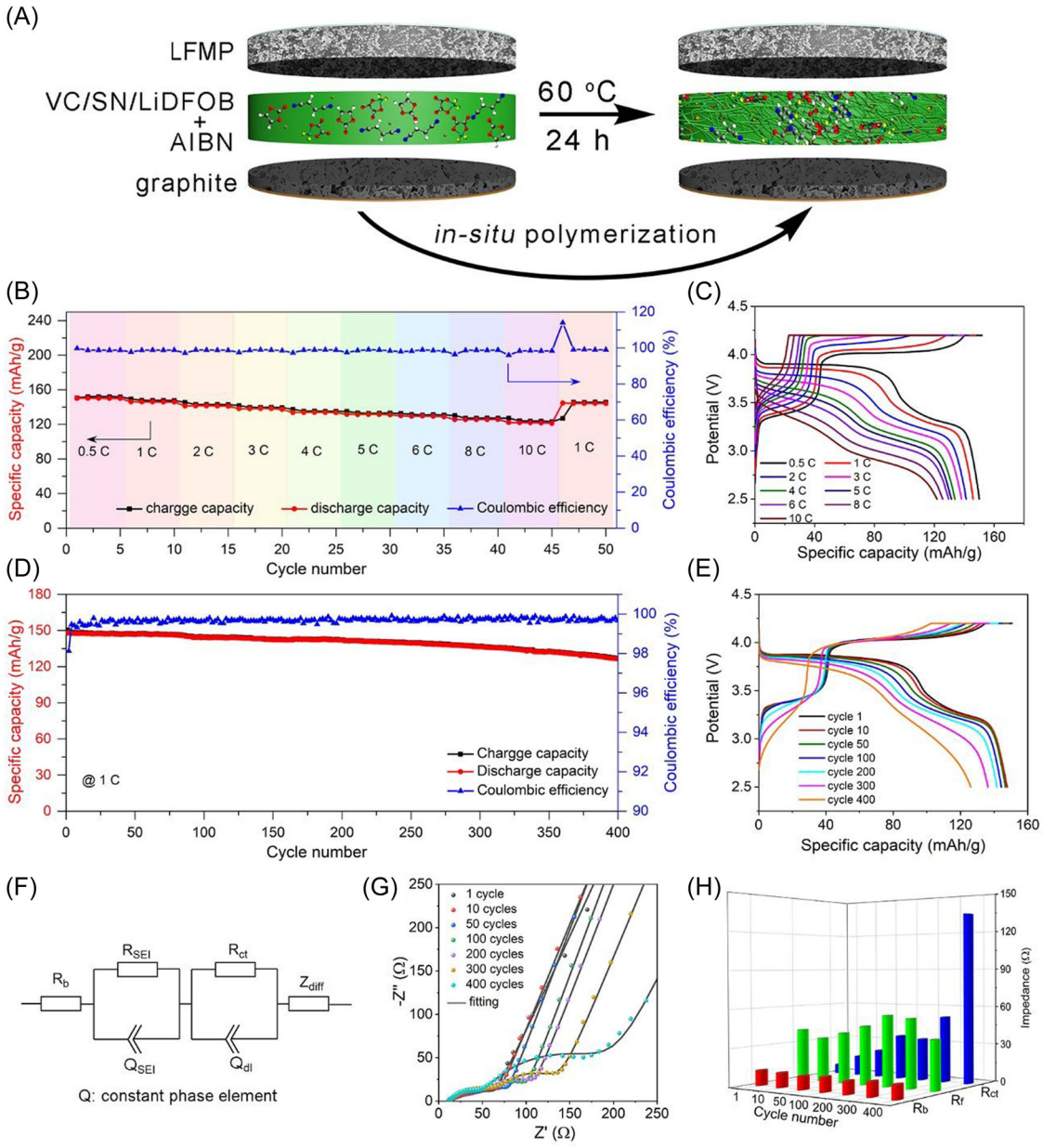

FIGURE 5 Battery performance of LFMP/PVCA–SN CPE/graphite battery. (A) Assembly diagram of lithium-ion full battery. (B) Charge/discharge curves and (C) specific capacity at varied current density. (D) Discharge specific capacity and Coulombic efficiency at 1 C. (E) Charge/discharge curves at varied cycle numbers. (F) An equivalent circuit was proposed for the analysis of an LFMP/PVCA–SN CPE/Li battery. The evolution of (G) Nyquist plots and (H) impedance date of LFMP/PVCA–SN CPE/Li battery at varied cycle numbers. AIBN, 2,2-azobisisobutyronitrile; CPE, composite polymer electrolyte; LFMP, $LiFe_{0.31}Mn_{0.69}PO_4$; LIDFOB, lithium difluoro(oxalato)borate; PVCA, polyvinylene carbonate; R_b, bulk resistance; R_{ct}, charge transference impedance; R_{SEI}, solid electrolyte interface; SN, succinonitrile; VC, vinylene carbonate; Z_{diff}, Warburg diffusion resistance.

this, LFMP/PVCA–SN CPE/graphite battery at 10 C afforded 81.2% of the capacity compared to that at 0.5 C, revealing the excellent rate performance of LFMP/PVCA–SN CPE/graphite battery. After the rate test, the reversible discharge capacity of the battery returned to 144.2 mAh/g at 1 C, which was close to the prior state. Compared with LFMP/PVCA–SN CPE/Li battery, LFMP/PVCA–SN CPE/graphite battery displayed a lower working potential, due to the relatively higher potential of graphite than lithium metal electrode. Even so, the high discharge platform of LFMP/PVCA–SN CPE/graphite battery was higher than 3.9 V (0.5 C), which was in parity with the universal $LiCoO_2$/graphite batteries.[21]

The long cycling performance of the LFMP/PVCA–SN CPE/graphite battery was also monitored. The battery was first cycled under a current density of 0.5 C six times to

activate the cathode and anode, followed by a current density of 1 C for long cycling. The battery showed an average Coulombic efficiency of over 99.7% (Figure 5D) at 1 C, and a 14.5% fade of capacity was detected over 400 cycles. In addition, the charge and discharge curves presented two obvious platforms all the time (Figure 5E). The superior charge/discharge performance of the LFMP/PVCA–SN CPE/graphite battery was ascribed to the stable PVCA–SN CPE and its excellent compatibility with electrodes.

EIS of LFMP/PVCA–SN CPE/graphite battery after varied cycles was conducted to analyze the evolution of impedance. The battery was galvanostatically discharged to 2.5 V and underwent a chronoamperometry process for 5 min. Two semicircles were observed in the electrochemical impedance spectroscopy (EIS) curves, which were related to solid–electrolyte interface (R_{SEI}) at a high-medium frequency and charge transference impedance (R_{ct}) at medium-low frequency, respectively. The equivalent circuit model was shown in Figure 5F, wherein, two parallel resistance and constant phase element systems were in series with bulk resistance (R_b) and Warburg diffusion resistance (Z_{diff}). Nyquist curves at varied cycle numbers and fitting curves based on the above equivalent circuit model were shown in Figure 5G. The fitting results showed that R_b exhibited no evident change during 400 cycles (Figure 5H), demonstrating the stable electrolyte system in the battery. The impedance related to the solid–electrolyte interface (R_{SEI}) accounted for a prominent proportion of the whole impedance, which was attributed to the electrochemical decomposition of electrolytes on the graphite anode. Even so, the change in R_{SEI} was not distinct. In contrast, the increase of R_{ct} was noticeable, increasing from 7.5 Ω after 1 cycle to 133.4 Ω after 400 cycles. The continuously increasing R_{ct} may be attributed to the electrochemical degradation of the LFMP cathode.

To understand further the degradation mechanism of LFMP/PVCA–SN CPE/graphite battery, the post-cycling electrodes were conducted by SEM, energy dispersive spectroscopy (EDS), and X-ray photoelectron spectroscopy. SEM of graphite showed that an unevenly thick SEI was covered on the surface of graphite (Figure 6A), leading to an increased impedance of batteries. EDS indicated that some Mn element was detected in graphite (Figure 6B), which originated in the LFMP cathode. Compound VC and PVCA can form an excellent interfacial with cathode and anode.[6a,12] The attenuation performance of LFMP/PVCA–SN CPE/graphite battery may be related to compound SN. Similar to most electrolyte systems, the SEI on graphite cathode was rich in LiF, Li_2CO_3, PVCA, and lithium alkyl carbonates (Figure 6B–E).[22] However, by-products of SN were also detected (Figure 6D). On the negative side, the triple bond cyano group would break and induce the polymerization of SN on the graphite anode.[23] However, on the

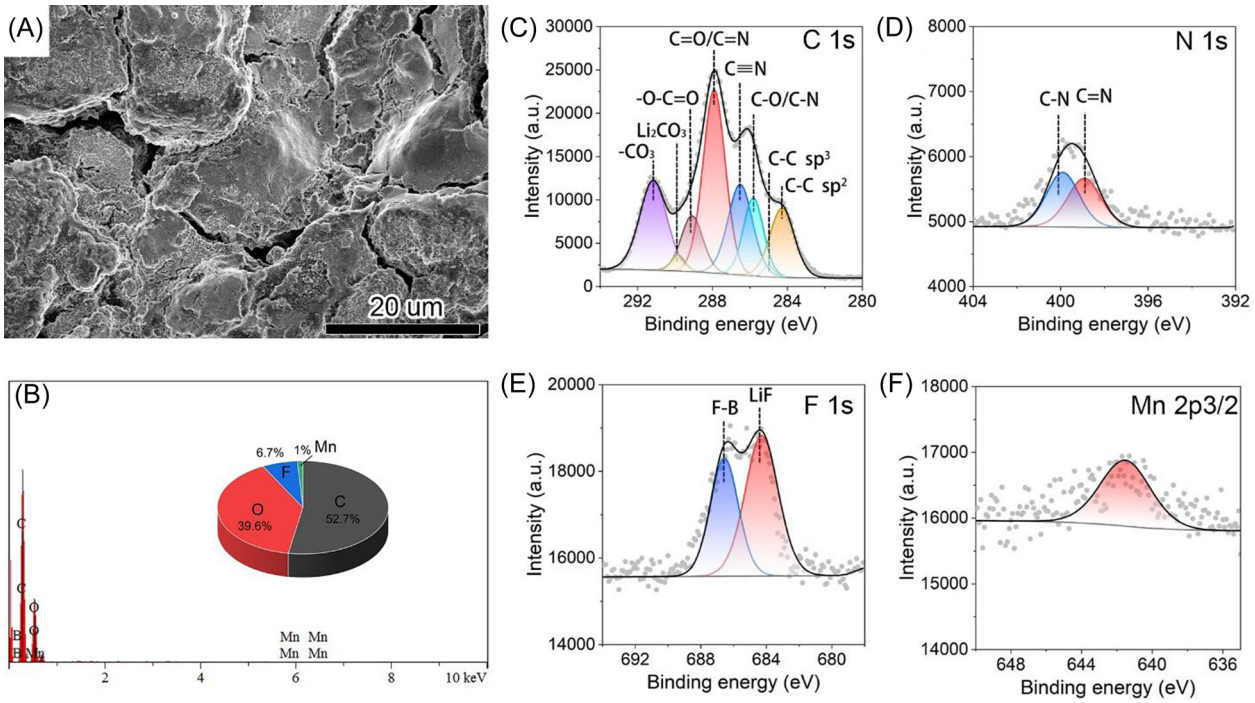

FIGURE 6 (A) Scanning electron microscope, (B) energy dispersive spectroscopy, and (C, D, E, F) X-ray photoelectron spectroscopy of cycled graphite anode.

positive side, the cyano group would combine with three Li ions to generate Li_3N (Supporting Information: Figure S15). In addition, the Mn 2p2/3 spectrum mainly consists of a strong peak from the Mn–O binder (~642 eV). The dissolution of the Mn element from the cathode not only caused the transformation of LFMP cathode materials but also damaged the SEI layer on graphite and lead to malignant SEI growth.[24] The introduction of chelating agents with Mn cation trapping to the designed electrolyte systems may be able to lead to performance improvements in LFMP/graphite full batteries.

4 | CONCLUSION

In this paper, a PVCA-based quasi solid-state composite polymer electrolyte via in situ polymerization process for ambient-temperature lithium-metal and lithium-ion batteries was demonstrated. In the proposed quasi solid-state composite polymer electrolyte, SN can plasticize the polymer electrolyte, coordinate with lithium-ion, and modulate the molecular weight of the polymer. Hence, SN was introduced as the multifunctional component to increase ionic conductivity. The PVCA–SN CPE showed an ionic conductivity of up to 4.5×10^{-4} S/cm, an electrochemical window of 4.36 V, a lithium-ion transference number of 0.21, and good interfacial compatibility with electrodes at 25°C. The assembled PVCA-based LFMP/graphite full battery demonstrated a good long cycling performance. The capacity decay of LFMP/PVCA–SN CPE/graphite battery mainly came from the following factors: (1) electrochemical decomposition of SN on cathode and anode and (2) dissolution of the Mn element from LFMP cathode caused by Jahn–Teller effect. Nevertheless, the proposition of PVCA-based quasi solid-state composite polymer electrolyte provides a resultful strategy for high-performance rechargeable lithium batteries. Furthermore, the pouch battery with a discharge capacity of 64.8 mAh showed a reliable safety performance. In addition, the similar assembly technology to liquid electrolyte-based lithium batteries demonstrated that PVCA–SN CPE provided an effective solution for next-generation high-performance lithium-ion batteries.

ACKNOWLEDGMENTS

This work was supported by the National Natural Science Foundation of China (Grant No. 51872127, Grant No. 22139001), the Key R&D Plan of Hubei Province (Grant No. 2020BAA030), and the Chutian Scholar Program of Hubei Province.

CONFLICT OF INTEREST STATEMENT

The authors declare no conflict of interest.

DATA AVAILABILITY STATEMENT

The data that support the findings of this study are available from the corresponding author upon reasonable request.

ORCID

Jingchao Chai http://orcid.org/0000-0003-4613-1316
Zhihong Liu http://orcid.org/0000-0002-3554-7992
Guanglei Cui http://orcid.org/0000-0003-1072-2819

REFERENCES

1. (a) Tarascon JM, Armand M. Issues and challenges facing rechargeable lithium batteries. *Nature*. 2001;414:359-367; (b) Liu Y, Zhu Y, Cui Y. Challenges and opportunities towards fast-charging battery materials. *Nat Energy*. 2019;4:540; (c) Zou P, Sui Y, Zhan H, et al. Polymorph evolution mechanisms and regulation strategies of lithium metal anode under multiphysical fields. *Chem Rev*. 2021;121(10):5986; (d) Zhou W, Li W, Gao J, et al. SnF_2 -catalyzed formation of polymerized dioxolane as solid electrolyte and its thermal decomposition behavior. *Angew Chem Int Ed*. 2022;61(6):e202114805.
2. (a) Wei Z, Chen S, Wang J, et al. A large-size, bipolar-stacked and high-safety solid-state lithium battery with integrated electrolyte and cathode. *J Power Sources*. 2018;394:57-66; (b) Liu J, Shen X, Zhou J, et al. Nonflammable and high-voltage-tolerated polymer electrolyte achieving high stability and safety in 4.9 V-class lithium metal battery. *ACS Appl Mater Interfaces*. 2019;11(48):45048-45056; (c) Zhang J, Zhao J, Yue L, et al. Safety-reinforced poly(propylene carbonate)-based all-solid-state polymer electrolyte for ambient-temperature solid polymer lithium batteries. *Adv Energy Mater*. 2015;5(24):1501082.
3. (a) Wang Q, Ping P, Zhao X, Chu G, Sun J, Chen C. Thermal runaway caused fire and explosion of lithium ion battery. *J Power Sources*. 2012;208:210-224; (b) Meng X, Yang K, Zhang M, et al. Experimental study on combustion behavior and fire extinguishing of lithium iron phosphate battery. *J Energy Storage*. 2020;30:101532; (c) Nagourney T, Jordan J, Marsh L, Scardino D, May BM. The implications of post-fire physical features of cylindrical 18650 lithium-ion battery cells. *Fire Technol*. 2021;57(4):1707-1722; (d) Yuan S, Chang C, Yan S, et al. A review of fire-extinguishing agent on suppressing lithium-ion batteries fire. *J Energy Chem*. 2021;62:262-280.
4. (a) Liang H-J, Gu Z-Y, Zhao X-X, et al. Advanced flame-retardant electrolyte for highly stabilized K-ion storage in graphite anode. *Sci Bull*. 2022;67(15):1581; (b) Qi S, Liu J, He J, et al. Structurally tunable characteristics of ionic liquids for optimizing lithium plating/stripping via electrolyte engineering. *J Energy Chem*. 2021;63:270; (c) Liang HJ, Gu ZY, Zhao XX, et al. Ether-based electrolyte chemistry towards high-voltage and long-life Na-ion full batteries. *Angew Chem Int Ed*. 2021;60(51):26837; (d) He J, Wang H, Zhou Q, et al. Unveiling the role of Li^+ solvation structures with commercial carbonates in the formation of solid

electrolyte interphase for lithium metal batteries. *Small Methods*. 2021;5(8):e2100441.

5. Zhao C-D, Guo J-Z, Gu Z-Y, et al. Flexible quasi-solid-state sodium-ion full battery with ultralong cycle life, high energy density and high-rate capability. *Nano Res*. 2021;15(2):925-932.
6. (a) Chai J, Liu Z, Ma J, et al. In situ generation of poly (vinylene carbonate) based solid electrolyte with interfacial stability for $LiCoO_2$ lithium batteries. *Adv Sci*. 2016;4(2): 1600377; (b) Zhang J, Zang X, Wen H, et al. High-voltage and free-standing poly(propylene carbonate)/$Li_{6.75}La_3Zr_{1.75}Ta_{0.25}O_{12}$composite solid electrolyte for wide temperature range and flexible solid lithium ion battery. *J Mater Chem A*. 2017;5(10):4940; (c) Cai D, Wang D, Chen Y, et al. A highly ion-conductive three-dimensional LLZAO-PEO/LiTFSI solid electrolyte for high-performance solid-state batteries. *Chem Eng J*. 2020;394:124993; (d) Lang J, Jin Y, Liu K, et al. High-purity electrolytic lithium obtained from low-purity sources using solid electrolyte. *Nat Sustain*. 2020;3:386-390.
7. (a) Zhou J, Ji H, Liu J, Qian T, Yan C. A new high ionic conductive gel polymer electrolyte enables highly stable quasi-solid-state lithium sulfur battery. *Energy Storage Mater*. 2019;22:256-264; (b) Yang S, Zhang Z, Lin J, et al. Recent progress in quasi/all-solid-state electrolytes for lithium–sulfur batteries. *Front Energy Res*. 2022;10:945003; (c) Lu J, Jaumaux P, Wang T, Wang C, Wang G. Recent progress in quasi-solid and solid polymer electrolytes for multivalent metal-ion batteries. *J Mater Chem A*. 2021;9(43): 24175-24194.
8. (a) Kato Y, Hori S, Kanno R. $Li_{10}GeP_2S_{12}$-type superionic conductors: synthesis, structure, and ionic transportation. *Adv Energy Mater*. 2020;10(42):2002153; (b) Kuhn A, Duppel V, Lotsch BV. Tetragonal $Li_{10}GeP_2S_{12}$ and Li_7GePS_8—exploring the Li ion dynamics in LGPS Li electrolytes. *Energy Environ Sci*. 2013;6(12):3548; (c) Wang CW, Ren FC, Zhou Y, et al. Engineering the interface between $LiCoO_2$ and $Li_{10}GeP_2S_{12}$ solid electrolytes with an ultrathin $Li_2CoTi_3O_8$ interlayer to boost the performance of all-solid-state batteries. *Energy Environ Sci*. 2021;14(1):437-450.
9. (a) Luo X, Wu X, Xiang J, et al. Heterovalent cation substitution to enhance the ionic conductivity of halide electrolytes. *ACS Appl Mater Interfaces*. 2021;13(40): 47610-47618; (b) Asano T, Sakai A, Ouchi S, Sakaida M, Miyazaki A, Hasegawa S. Solid halide electrolytes with high lithium-ion conductivity for application in 4 V class bulk-type all-solid-state batteries. *Adv Mater*. 2018;30(44):1803075; (c) Li X, Liang J, Chen N, et al. Water-mediated synthesis of a superionic halide solid electrolyte. *Angew Chem Int Ed*. 2019;58(46):16427-16432.
10. (a) Wen SJ, Richardson TJ, Ghantous DI, Striebel KA, Ross PN, Cairns EJ. FTIR characterization of PEO + LiN$(CF_3SO_2)_2$ electrolytes. *J Electroanal Chem*. 1996;408(1): 113-118; (b) Xu S, Sun Z, Sun C, et al. Homogeneous and fast ion conduction of PEO-based solid-state electrolyte at low temperature. *Adv Funct Mater*. 2020;30(51):2007172; (c) Shi Y, Fan Z, Ding B, et al. Atomic-scale Al_2O_3 modified PEO-based composite polymer electrolyte for durable solid-state Li−S batteries. *J Electroanaly Chem*. 2021;881:114916; (d) Wang H, Lin C, Yan X, et al. Mechanical property-reinforced PEO/PVDF/$LiClO_4$/SN blend all solid polymer electrolyte for lithium ion batteries. *J Electroanal Chem*. 2020;869:114156; (e) Li Z, Zhang S, Jiang Z, Cai D, Gu C, Tu J. Deep eutectic solvent-immobilized PVDF-HFP eutectogel as solid electrolyte for safe lithium metal battery. *Mater Chem Phys*. 2021; 267:124701; (f) Lopez J, Gonzalez R, Ayala J, et al. Centrifugally spun TiO_2/C composite fibers prepared from TiS_2/PAN precursor fibers as binder-free anodes for LIBS. *J Phys Chem Solids*. 2021;149:109795; (g) Xiang J, Zhang Y, Zhang B, et al. A flame-retardant polymer electrolyte for high performance lithium metal batteries with an expanded operation temperature. *Energy Environ Sci*. 2021;14(6): 3510-3521; (h) Wang Y, Xu R, Xiao B, et al. A poly(1,3-dioxolane) based deep-eutectic polymer electrolyte for high performance ambient polymer lithium battery. *Mater Today Phys*. 2022;22:100620.
11. (a) Yan M, Qu W, Su Q, et al. Biodegradable bacterial cellulose-supported quasi-solid electrolyte for lithium batteries. *ACS Appl Mater Interfaces*. 2020;12(12):13950-13958; (b) Ding J, Xu R, Yan C, et al. Integrated lithium metal anode protected by composite solid electrolyte film enables stable quasi-solid-state lithium metal batteries. *Chin Chem Lett*. 2020;31(9):2339-2342.
12. Chai J, Liu Z, Zhang J, et al. A superior polymer electrolyte with rigid cyclic carbonate backbone for rechargeable lithium ion batteries. *ACS Appl Mater Interfaces*. 2017;9(21): 17897-17905.
13. Liu Z, Chai J, Xu G, Wang Q, Cui G. Functional lithium borate salts and their potential application in high performance lithium batteries. *Coord Chem Rev*. 2015;292:56-73.
14. Wang C, Zhang H, Li J, Chai J, Dong S, Cui G. The interfacial evolution between polycarbonate-based polymer electrolyte and Li-metal anode. *J Power Sources*. 2018;397:157-161.
15. (a) Alarco PJ, Abu-Lebdeh Y, Abouimrane A, Armand M. The plastic-crystalline phase of succinonitrile as a universal matrix for solid-state ionic conductors. *Nat Mater*. 2004;3(7): 476-481; (b) Echeverri M, Kim N, Kyu T. Ionic conductivity in relation to ternary phase diagram of poly(ethylene oxide), succinonitrile, and lithium bis(trifluoromethane)sulfonimide blends. *Macromolecules*. 2012;45(15):6068-6077; (c) Polu AR, Rhee HW, Kim DK. New solid polymer electrolytes (PEO_{20}–LiTDI–SN) for lithium batteries: structural, thermal and ionic conductivity studies. *J Mater Sci Mater Electron*. 2015;26(11): 8548-8554; (d) Lyu W, He G, Liu T. PEO-LITFSI-SiO_2-SN system promotes the application of polymer electrolytes in all-solid-state lithium-ion batteries. *ChemistryOpen*. 2020;9(6): 713-718.
16. Hu Z, Xian F, Guo Z, et al. Nonflammable nitrile deep eutectic electrolyte enables high-voltage lithium metal batteries. *Chem Mater*. 2020;32(8):3405-3413.
17. (a) Chen L, Wang K, Xie X, Xie J. Effect of vinylene carbonate (VC) as electrolyte additive on electrochemical performance of Si film anode for lithium ion batteries. *J Power Sources*. 2007;174(2): 538-543; (b) El Ouatani L, Dedryvère R, Siret C, et al. The effect of vinylene carbonate additive on surface film formation on both electrodes in Li-ion batteries. *J Electrochem Soc*. 2009;156(2): A103-A113; (c) Zampardi G, La Mantia F, Schuhmann W. In-operando evaluation of the effect of vinylene carbonate on the insulating character of the solid electrolyte interphase. *Electrochemis Commun*. 2015;58:1-5.

18. Chai J, Chen B, Xian F, et al. Dendrite-free lithium deposition via flexible-rigid coupling composite network for $LiNi_{0.5}Mn_{1.5}O_4$/Li metal batteries. *Small*. 2018;14(37):1802244.
19. Zeng X-X, Yin Y-X, Li N-W, Du WC, Guo YG, Wan LJ. Reshaping lithium plating/stripping behavior via bifunctional polymer electrolyte for room-temperature solid Li metal batteries. *J Am Chem Soc*. 2016;138(49):15825-15828.
20. Rosenwinkel MP, Schönhoff M. Lithium transference numbers in PEO/LiTFSA electrolytes determined by electrophoretic NMR. *J Electrochem Soc*. 2019;166(10):A1977-A1983.
21. (a) Deng Y, Kang T, Ma Z, et al. Safety influences of the Al and Ti elements modified $LiCoO_2$ materials on $LiCoO_2$/graphite batteries under the abusive conditions. *Electrochim Acta*. 2019;295:703-709; (b) Deng Y, Wang Z, Ma Z, Nan J. Positive-temperature-coefficient graphite anode as a thermal runaway firewall to improve the safety of $LiCoO_2$/graphite batteries under abusive conditions. *Energy Technol*. 2020;8(3):1901037; (c) Wang DY, Sinha NN, Petibon R, Burns JC, Dahn JR. A systematic study of well-known electrolyte additives in $LiCoO_2$graphite pouch cells. *J Power Sources*. 2014;251:311-318; (d) He YB, Li B, Yang QH, et al. Effects of current densities on the formation of $LiCoO_2$/graphite lithium ion battery. *J Solid State Electrochem*. 2011;15(9):1977-1985.
22. (a) Heiskanen SK, Kim J, Lucht BL. Generation and evolution of the solid electrolyte interphase of lithium-ion batteries. *Joule*. 2019;3(10):2322-2333; (b) Ryou M-H, Lee J-N, Lee DJ, et al. Effects of lithium salts on thermal stabilities of lithium alkyl carbonates in SEI layer. *Electrochim Acta*. 2012;83:259-263; (c) Ota H, Sakata Y, Inoue A, Yamaguchi S. Analysis of vinylene carbonate derived SEI layers on graphite anode. *J Electrochem Soc*. 2004;151(10):A1659-A1669; (d) Zane D, Antonini A, Pasquali M. A morphological study of SEI film on graphite electrodes. *J Power Sources*. 2001;97-98:146-150.
23. Dong R, Zheng J, Yuan J, et al. A polyethylene oxide/metal-organic framework composite solid electrolyte with uniform Li deposition and stability for lithium anode by immobilizing anions. *J Colloid Interface Sci*. 2022;620:47-56.
24. Banerjee A, Ziv B, Luski S, Aurbach D, Halalay IC. Increasing the durability of Li-ion batteries by means of manganese ion trapping materials with nitrogen functionalities. *J Power Sources*. 2017;341:457-465.

SUPPORTING INFORMATION

Additional supporting information can be found online in the Supporting Information section at the end of this article.

How to cite this article: Liu Z, Zhang S, Zhou Q, et al. Insights into quasi solid-state polymer electrolyte: the influence of succinonitrile on polyvinylene carbonate electrolyte in view of electrochemical applications. *Battery Energy*. 2023;2:20220049. doi:10.1002/bte2.20220049